A bipolar host containing 1,2,3-triazole for realizing highly efficient phosphorescent organic light-emitting diodes

Myoung Ki Kim, Jongchul Kwon, Tae-Hyuk Kwon and Jong-In Hong*

Received (in Montpellier, France) 4th February 2010, Accepted 22nd March 2010
First published as an Advance Article on the web 27th April 2010
DOI: 10.1039/c0nj00091d

We have developed a novel host material, 9,9′-(2-((4-phenyl-1,2,3-triazol-1-yl)methyl)biphenyl-4,4′-diyl)biscarbazole (**CBP-TA**), for realizing highly efficient blue phosphorescent OLEDs. The maximum external quantum efficiency of the OLED device developed using **CBP-TA** doped with a blue phosphorescent material was 30% greater than that of a **CBP**-based device. This enhanced external quantum efficiency resulted from the bipolar properties of the new host, owing to which well-balanced hole and electron transport through the emitting layer was achieved. The excellent bipolar carrier transport properties of the new host were experimentally verified using various OLED device data.

Introduction

Organic light-emitting diodes (OLEDs) have attracted considerable attention owing to a number of advantages, such as high brightness, high contrast, low power consumption, low cost,[1,2] and a wide range of applications in full-color flat-panel displays and solid-state lighting.[3,4] In particular, phosphorescent materials are more attractive compared to fluorescent materials as they can reach an internal quantum efficiency of 100% through the radiative recombination of both singlet and triplet excitons. Highly efficient blue-emitting materials still need to be developed if high performance OLEDs are to be commercialized. Efficient blue-emitting materials are important not only as blue emitters themselves but also as hosts for other emitters, particularly in phosphorescent OLEDs.[5–8]

In order to improve phosphorescent blue emission, it is vital to prevent reverse energy transfer from the emitter back to the host and to effectively confine triplet excitons to the triplet emitter molecules. This can be achieved by ensuring that the triplet excited state of the host material is higher than that of the triplet emitter.[9] An alternative method for improving the performance of OLEDs is to use bipolar host materials. Bipolar host materials contribute to the balanced transport of carriers to the triplet emitter and help increase the probability of carrier recombination.[10,11]

Carbazole derivatives have been utilized in the construction of highly photoconductive amorphous organic materials and thus have been used as hole transport materials in OLEDs *via* radical cation species or as host materials.[12] Due to its high triplet energy (*ca.* 3.0 eV), carbazole is a good candidate for a blue phosphorescent host material. However, carbazole is a well-known electron donor. This may result in unbalanced carrier injection and transport into the emitting layer, thus limiting device performance.[13]

Department of Chemistry, College of Natural Sciences, Seoul National University, Seoul 151-747, Korea. E-mail: jihong@snu.ac.kr; Fax: +82 2-889-1568; Tel: +82 2-880-6682

To overcome these issues, we designed a unique bipolar host material, 9,9′-(2-((4-phenyl-1,2,3-triazol-1-yl)methyl)biphenyl-4,4′-diyl)biscarbazole (**CBP-TA**), that is obtained by coupling 4,4′-*N*,*N*′-dicarbazolebiphenyl (**CBP**; an electron donor) and 1,2,3-triazole (an electron acceptor with a high electron affinity). The external quantum efficiency (EQE) when **CBP-TA** was used as the host for iridium(III) bis(4,6-(difluorophenyl)-pyridinato-*N*,*C*2′) picolinate(FIrpic) blue phosphorescent OLEDs was 30% greater than the EQE when **CBP** alone was used as the host. The FIrpic-doped **CBP-TA** device exhibited a stable blue emission at Commission Internationale de l'Eclairage (CIE) coordinates of (0.17, 0.35) with a high current efficiency of 9.0 cd A^{-1} and a power efficiency of 6.9 lm W^{-1}. The efficiency of the FIrpic-doped **CBP-TA** device was higher than that of the FIrpic-doped **CBP** device. The increased OLED efficiency results from the bipolar properties of **CBP-TA**.

Results and discussion

The molecular structure of **CBP-TA** is shown in Scheme 1. **CBP-TA** was synthesized according to Scheme 2.

Fig. 1a shows the UV absorption of **CBP-TA**, and photoluminescence (PL) spectra at 293 and 77 K of **CBP** and **CBP-TA** in 2-methyltetrahydrofuran. The fluorescence emission maximum wavelengths of **CBP** and **CBP-TA** appear at 365 and 362 nm, respectively, and the phosphorescence

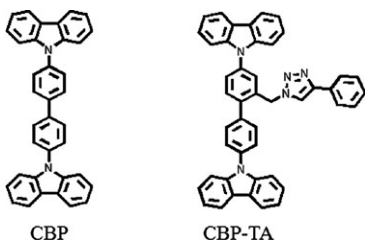

Scheme 1 The molecular structures of **CBP** (left) and **CBP-TA** (right).

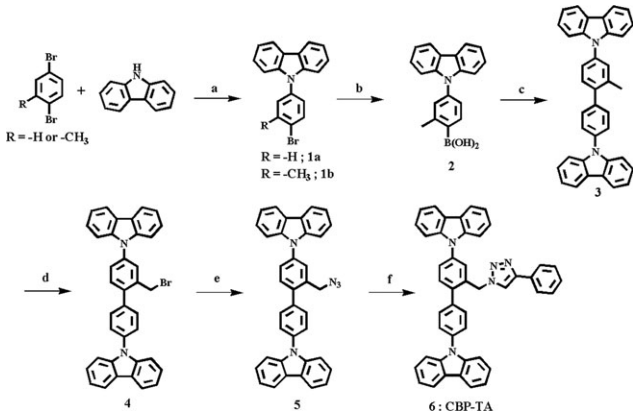

Scheme 2 The synthesis of **CBP-TA**: (a) CuI, K_3PO_4, (±)-*trans*-1,2-diaminocyclohexane, toluene; (b) n-BuLi, trimethylborate, THF; (c) **1a**, Na_2CO_3, 2-dicyclohexylphosphino-2′-methylbiphenyl, tris-(dibenzylidene acetone)dipalladium(0), toluene; (d) NBS, CCl_4; (e) NaN_3, DMF; (f) phenyl acetylene, $Cu(SO_4)_2$, L-ascorbic acid sodium salt, THF, H_2O.

triplet emission of **CBP** and **CBP-TA** appears at 454 and 439 nm, respectively, which was determined by taking the first emission peak of phosphorescence as the transition energy of $T_1 \rightarrow S_0$.[14] The triplet emission (triplet energy 2.71 eV, the arrow in Fig. 1b) of **CBP-TA** is blue-shifted compared to that of **CBP** (triplet energy 2.56 eV). The PL spectrum of **CBP-TA** shows a blue shift at 293 and 77 K compared to that of **CBP** because of the electron deficient 1,2,3-triazole unit, indicating an increase in the singlet–triplet band gap (Fig. 1b).

The HOMO energy value of **CBP-TA** was estimated by cyclic voltammetry (CV). This electrochemical experiment was referenced with respect to a silver wire as the quasi-reference electrode (AgQRE) at room temperature and then calibrated to a standard hydrogen electrode (SHE) using ferrocene (Fc/Fc^+). Acetonitrile solutions for CV contained a 2 mm diameter Pt working electrode, a Pt counterelectrode and a 0.1 M $TBAPF_6$ (tetra-n-butylammoniumhexafluorophosphate) supporting electrolyte. The oxidation potential of **CBP-TA** was observed at $E_{1/2}$ = 1.51 V *vs.* SHE. The HOMO energy level of **CBP-TA** (−6.00 eV) was calculated from $E_{1/2}$ after correction of the vacuum energy level (4.49 eV). The LUMO level of **CBP-TA**, which was determined from the HOMO level and the cross section wavelength between the absorption and emission spectra, is 2.5 eV. The HOMO and LUMO levels of **CBP** were determined to be 5.9 and 2.6 eV, respectively. These electrochemical data confirm that the presence of the 1,2,3-triazole unit leads to an increase in the energy band gap.

In order to evaluate the electroluminescence (EL) and charge transporting properties of **CBP-TA**, we designed several OLED device structures, which are described in Table 1. Organic layers were fabricated by high vacuum (10^{-7} torr) thermal evaporation onto a patterned ITO glass pre-cleaned in a UV-ozone chamber. A 10 nm-thick film of copper phthalocyanine (CuPc) and a 30 nm-thick film of 4,4′-bis[*N*-(1-naphthyl)-*N*-phenyl-amino]-biphenyl (α-NPD) served as the hole injection layer (HIL) and hole transport layer (HTL), respectively. The emitting layer (EML) was prepared by co-evaporating the **CBP** or **CBP-TA** host and 6 wt% FIrpic

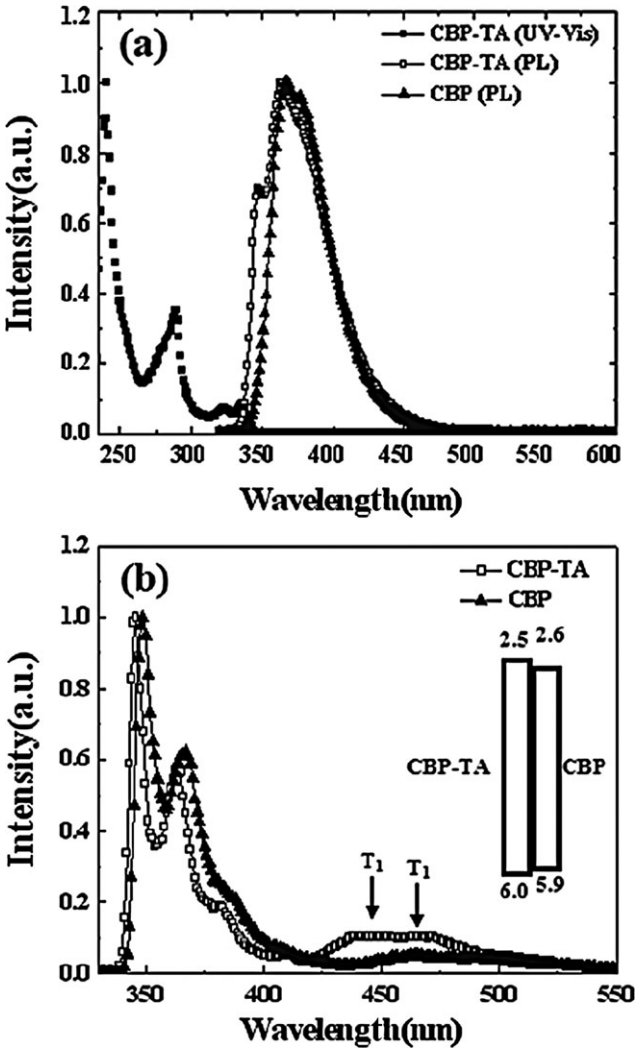

Fig. 1 (a) Optical absorption spectra and PL spectra of **CBP-TA** and **CBP** at 293 K. (b) PL spectra of **CBP-TA** and **CBP** at 77 K; the inset shows the energy band gap of **CBP-TA** and **CBP**.

dopant. Next, a 30 nm-thick 4-biphenyloxolatoaluminium(III)-bis(2-methyl-8-quinolinato)4-phenylphenolate (Balq) layer, functioning as both a hole blocking layer (HBL) and an electron transporting layer (ETL), was deposited; this was then followed by the deposition of LiF as an electron injection layer (EIL). Finally, after changing the metal mask, a 100 nm-thick aluminium film was deposited on the EIL and then encapped. A Keithly 2400 source meter attached to a computer was used to operate the device.

First, we examined devices 1 and 2, having **CBP-TA** or **CBP** as the host for FIrpic, which was sandwiched between the HTL and ETL.[15] The maximum efficiencies of devices 1 and 2 were 5.4% (9.2 cd A^{-1}) and 4.2% (7.5 cd A^{-1}), respectively. Both devices exhibited a bright blue emission with a peak at 472 nm from the emission of FIrpic at CIE coordinates of (0.17, 0.35). It is important to note that the current density of device 1 was less than that of device 2; this can be explained by the higher charge injection barrier of **CBP-TA** compared to that of **CBP** (Fig. 1b). However, the luminance and efficiency of device 1 were higher than those of device 2 (Fig. 2). We

Table 1 Layer structures and EL performance data of the OLED devices (units: nm)

Device[a]	EML	ETL	Turn-on voltage/V[b]	Q. E. (%)[c]	P. E./ lm W^{-1}[d]	C. E./ cd A^{-1}[e]	Emission peaks/ nm	CIE coordinates
1	**CBP-TA**: 6% Firpic (30)	Balq (30)	4.6	5.4	6.9	9.0	472, 500	(0.17, 0.35)
2	**CBP**: 6% Firpic (30)	Balq (30)	4.2	4.2	6.4	7.5	472, 500	(0.17, 0.35)
3	**CBP-TA**: 6% Firpic (60)	Alq_3 (30)	n.d.[f]	—	—	—	472, 500	(0.18, 0.34)
4	**CBP**: 6% Firpic (60)	Alq_3 (30)	—	n.d.	—	—	472, 500, 530	(0.22, 0.41)
5	**CBP-TA**: 6% Firpic (30)	**CBP-TA** (20)/Alq_3 (30)	—	—	n.d.	—	472, 500	(0.21, 0.36)
6	**CBP**: 6% Firpic (30)	**CBP** (20)/Alq_3 (30)	—	—	—	n.d.	472, 500, 530	(0.30, 0.44)
7	**CBP-TA**: 6% $Ir(ppy)_3$ (30)	Balq (30)	5.0	7.2	6.5	19.9	512	(0.32, 0.61)
8	**CBP**: 6% $Ir(ppy)_3$ (30)	Balq (30)	4.8	3.7	3.3	10.2	512	(0.32, 0.61)

[a] Device structure of 1–8: CuPc (10 nm)/NPD (30 nm)/EML/ETL/LiF (1 nm)/Al (100 nm). [b] Voltage at 1 cd. [c] Maximum quantum efficiency. [d] Maximum power efficiency. [e] Maximum luminance efficiency. [f] Not determined. We fabricated devices 3–6 for the purpose of comparing emission peaks and CIEs with those of **CBP**-based devices.

expected the performance of device 1 to be better than that of device 2 owing to the improved carrier balance in device 1. The improved carrier balance of device 1 is due to the bipolar properties of **CBP-TA**, which consists of both electron donor and electron acceptor units.[14,16] The efficiency of the examined devices may be lower than that of phosphorescent OLED devices fabricated using other hosts;[9–11,13,16] this is because, in the current study, we only compared the performance of devices 1 and 2, which comprised **CBP-TA** and **CBP**, respectively, as the hosts in order to confirm whether the bipolar host **CBP-TA** contributed to the device performance. In order to verify the bipolar carrier transport properties of **CBP-TA**, we fabricated devices 3 and 4, in which Alq_3 was used as the ETL instead of Balq. Fig. 3a shows the normalized EL spectra of devices 3 and 4 at identical driving voltages. The EL spectrum of device 4 includes three peaks, two at 472 and 500 nm due to FIrpic emission, and one at 530 nm due to Alq_3 emission, at CIE coordinates of (0.22, 0.41). This indicates that some of the electrons do not penetrate the **CBP** layer, because of which carrier recombination occurs at Alq_3.[13] In contrast, the EL spectrum of device 3 shows only two peaks at 472 and 500 nm, which are attributed to FIrpic emission at CIE coordinates of (0.17, 0.34). This is because carrier recombination occurs mainly in the EML, indicating the strong bipolar properties of **CBP-TA** and the well-balanced hole and electron transport through **CBP-TA** (Fig. 3a).[13,17]

To further investigate the bipolar properties of **CBP-TA**, we fabricated devices 5 and 6, in which **CBP-TA** and **CBP**, respectively, were inserted between EML and Alq_3. In the case of device 6, we observed an emission from Alq_3 because of a small degree of carrier recombination at Alq_3. On the other hand, in the case of device 5, no emission from Alq_3 was observed and an emission from FIrpic was predominant, thereby indicating that most of the electrons penetrated the **CBP-TA** layer and little carrier recombination had occurred at Alq_3 (Fig. 3b). This confirms that **CBP-TA** has excellent bipolar properties and therefore contributes significantly to

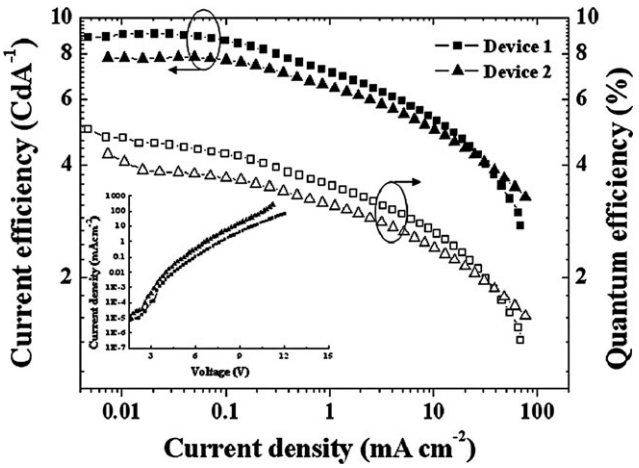

Fig. 2 Plots of current efficiency *vs.* current density for devices 1 and 2; the inset shows the plot of current density *vs.* voltage for devices 1 and 2.

the balanced transport of holes and electrons in OLED devices.[14,17]

To further verify the well-balanced hole and electron transport through **CBP-TA**, we fabricated an electron-only device with the structure ITO/**CBP** or **CBP-TA**/Balq/LiF/Al. As shown in Fig. 4, the turn-on voltage of the **CBP-TA**-based device is higher than that of the **CBP**-based device, and the current density of the **CBP-TA**-based device is less than that of the **CBP**-based device because of the higher charge injection barrier of **CBP-TA**. However, the luminance *vs.* current density of the **CBP-TA**-based device is higher than that of the **CBP**-based device. This result indicates that although **CBP-TA** reduces the charge injection capability, **CBP-TA** contributes to the balanced transport of holes and electrons because of its bipolar properties.[17]

It is well known that to enhance the performance of OLEDs, the triplet excited state of the host material should

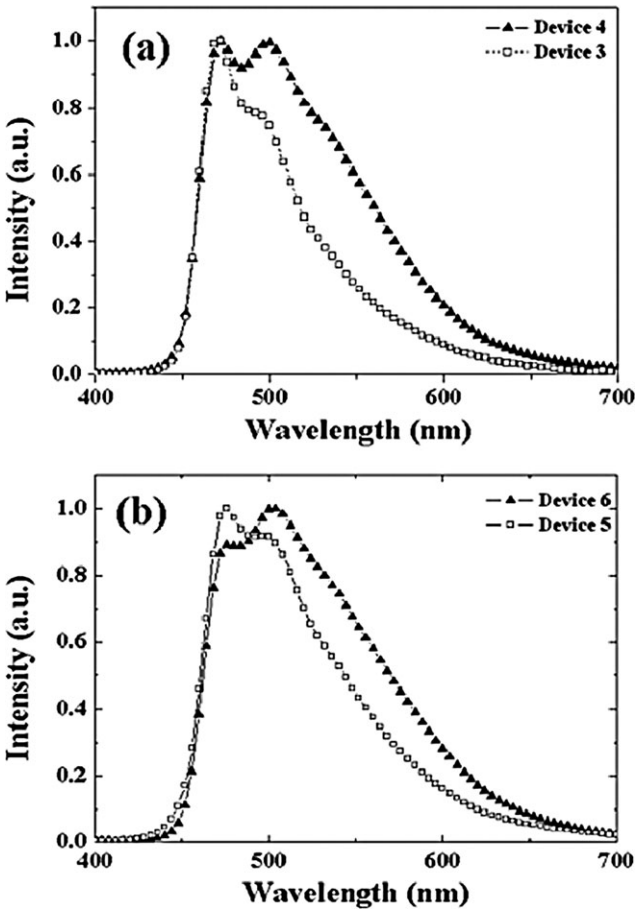

Fig. 3 (a) EL spectra of devices 3 and 4. (b) EL spectra of devices 5 and 6.

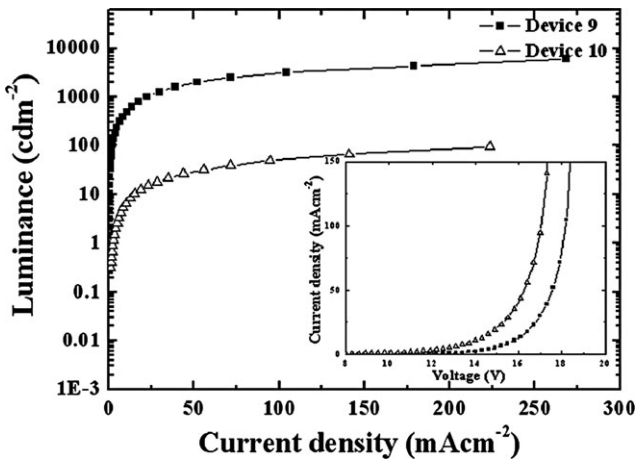

Fig. 4 Plots of current luminance *vs*. current density for devices 9 and 10; the inset shows the plots of current density *vs*. voltage for devices 9 and 10. Device 9: ITO/**CBP-TA** (30 nm)/Balq (20 nm)/LiF (1 nm)/Al (100 nm). Device 10: ITO/**CBP** (30 nm)/Balq (20 nm)/LiF (1 nm)/Al (100 nm).

be higher than that of the phosphorescent emitter.[9] Moreover, the **CBP-TA**-based device might show a better performance than the **CBP**-based device because the triplet excited state of **CBP-TA** (2.71 eV) is higher than that of **CBP** (2.56 eV).[16] In order to demonstrate that the high efficiency of the **CBP-TA**-based device results from the bipolar properties of **CBP-TA**, and not from its high triplet excited state, we fabricated devices 7 and 8 using *fac*-tris(2-phenylpyridine)-iridium ($Ir(ppy)_3$) instead of FIrpic. Since the triplet excited state of $Ir(ppy)_3$ is 2.4 eV,[18] reverse energy transfer from phosphorescent emitter $Ir(ppy)_3$ to the **CBP** host was prevented. Thus, the triplet excited state, which is lower for **CBP** compared to **CBP-TA**, does not significantly contribute to a decrease in device efficiency. Nevertheless, the emission efficiency of device 7 (19.9 cd A^{-1}), which comprises **CBP-TA**, is approximately twice that of device 8 (10.2 cd A^{-1}), which comprises **CBP**. This implies that the higher efficiency of device 7 results not only from a higher triplet excited state but also from the stronger bipolar properties of **CBP-TA** compared to those of **CBP**.

While 1,2,3-triazole provides **CBP-TA** with better bipolar properties, the CV data revealed that **CBP-TA** is electrochemically less stable than **CBP**. Also, the OLED device based on **CBP-TA** is less stable that the **CBP**-based OLED device. It is very likely that the introduction of a methylene linkage or/and a triazole unit into **CBP** reduces the electrochemical stability of **CBP-TA**.

Conclusion

In summary, we have synthesized a unique bipolar host material, **CBP-TA**, which was obtained by coupling **CBP** and 1,2,3-triazole. The EQE of the FIrpic-based blue phosphorescent OLEDs increased by 30% when **CBP-TA** was used as the host instead of **CBP**. This is because the new host exhibited excellent bipolar properties, owing to which well-balanced hole and electron transport through the emitting layer were achieved. These excellent bipolar transport properties and the resulting high performance of the device containing **CBP-TA** as the host suggest that efficient and versatile host materials for high performance OLEDs can be generated by coupling an electron donor with an electron acceptor.

Experimental section

Synthesis

^1H and ^{13}C NMR spectra were recorded using an Bruker Avance 300 MHz spectrometer in $CDCl_3$. ^1H NMR chemical shifts in $CDCl_3$ were referenced to $CHCl_3$ (7.27 ppm), and ^{13}C NMR chemical shifts in $CDCl_3$ reported relative to $CHCl_3$ (77.23 ppm). UV-vis spectra were recorded on a Beckman DU650 spectrophotometer. Fluorescence spectra were recorded on a Jasco FP-7500 spectrophotometer. Mass spectra were obtained using a MALDI-TOF MS from Bruker. High resolution masses were measured by FAB mass using a JEOL HP 5890 series instrument. Analytical thin layer chromatography was performed using Kieselgel 60F-254 plates from Merck. Column chromatography was carried out on Merck silica gel 60 (70–230 mesh). All solvents and reagents were commercially available and used without further purification unless otherwise noted.

9-(4-Bromo-3-methyl-phenyl)-9*H*-carbazole (1b). To a screw-capped test tube were added CuI (0.46 g, 0.24 mmol), carbazole (2.949 g, 17 mmol), K_3PO_4 (7.74 g, 30 mmol) and toluene, followed by nitrogen bubbling for 10–20 min. 2,5-Dibromotoleune (5 g, 20 mmol) and (±)-*trans*-1,2-diamino-cyclohexane (0.48 ml, 3.9 mmol) were then successively added under a stream of nitrogen. The reaction tube was sealed and the contents stirred while being heating in an oil bath at 110 °C for 24 h. The reaction mixture was cooled to ambient temperature, diluted with ethyl acetate (2–3 mL) and filtered through a plug of Celite®, eluting with additional ethyl acetate (10–20 mL). The filtrate was concentrated and the resulting residue purified by column chromatography, eluting with methylene chloride and hexane. Yield: 4.62 g, 81%. ^{1}H NMR (300 MHz, acetone-d_6): δ (ppm) 8.20 (d, 9 Hz, 2H), 7.88 (d, 9 Hz, 1H), 7.63 (s, 1H) 7.45–7.43 (m, 5H), 7.43–7.29 (m, 2H), 2.54 (s, 3H).

9-(4-Bromophenyl)-9*H*-carbazole (1a). To a screw-capped test tube were added CuI (0.650 mg, 0.31 mol), carbazole (3.54 g, 2 mmol), K_3PO_4 (10.24 g, 4 mol) and toluene, followed by nitrogen bubbling for 10–20 min. 1,4-Dibromobenzene (5 g, 21.2 mmol) and (±)-*trans*-1,2-diaminocyclohexane (0.637 ml, 5.2 mmol) were then successively added under a stream of nitrogen. The reaction tube was sealed and the contents stirred while being heating in an oil bath at 110 °C for 24 h. The reaction mixture was cooled to ambient temperature, diluted with ethyl acetate (2–3 mL) and filtered through a plug of Celite®, eluting with additional ethyl acetate (10–20 mL). The filtrate was concentrated and the resulting residue purified by column chromatography, eluting with methylene chloride and hexane. Yield: 5.53 g, 83%. ^{1}H NMR (300 MHz, DMSO-d_6): δ (ppm) 8.25 (d, 9 Hz, 2H), 7.86 (d, 9 Hz, 2H), 7.61 (d, 9 Hz, 2H), 7.42 (m, 4H), 7.30 (m, 2H).

4-Carbazol-9-yl-2-methyl-phenyl-4-boronic acid (2). To a stirred solution of **1b** (3 g, 8.54 mmol) in dry THF under N_2, cooled with dry ice and an acetone bath, was added n-BuLi (5.21 ml, 0.1 mmol) dropwise. After completion of the addition, the orange mixture was stirred 15 min and trimethyl borate (28.6 ml, 20 mmol) added. The reaction flask was kept in the cooling bath for 30 min and then allowed to warm to room temperature. 3 h later, the solvent was removed by evaporation under reduced pressure. Next, 1 N HCl was added and stirred for 30 min. The solvent was evaporated and the residues separated by flash column chromatography, eluting with methylene chloride and methanol. Yield: 1.3 g, 50%. ^{1}H NMR (300 MHz, DMSO-d_6): δ (ppm) 8.25 (d, 9 Hz, 2H), 7.86 (d, 9 Hz, 2H), 7.61 (d, 9 Hz, 2H), 7.42 (m, 4H), 7.30 (m, 2H).

9,9′-(2-Methyl)biphenyl-4,4′-diyl)biscarbazole (3). To a screw-capped test tube were added **2** (0.939 mg, 2.9 mmol), **1a** (1 g, 2.97 mmol), Na_2CO_3 (2.051 g, 90 mmol) and toluene, followed by nitrogen bubbling for 10–20 min. 2-Dicyclohexyl-phosphino-2′-methylbiphenyl (0.12 mmol) and tris(dibenzylidene acetone)dipalladium(0) (0.135 mg, 0.43 mmol) were then successively added under a stream of nitrogen. The reaction tube was quickly sealed and the contents stirred while being heated in an oil bath at 110 °C for 24 h. The reaction mixture was cooled to ambient temperature, diluted with ethyl acetate (2–3 mL) and filtered through a plug of Celite®, eluting with additional ethyl acetate (10–20 mL). The filtrate was concentrated and the resulting residue purified by column chromatography, eluting with methylene chloride and hexane. Yield: 1.54 g, 37%. ^{1}H NMR (300 MHz, acetone-d_6): δ (ppm) 8.26 (d, 9 Hz, 4H), 7.88–7.80 (m, 4H), 7.74–7.64 (m, 3H), 7.58–7.49 (m, 8H), 7.36–7.31 (t, 4H), 2.58 (s, 3H).

9,9′-(2-Bromomethyl)biphenyl-4,4′-diyl)biscarbazole (4). A mixture of 9,9′-(2-methyl)biphenyl-4,4′-diyl)biscarbazole (0.3 g, 0.6 mmol), NBS (0.138 g, 0.7 mmol) and AIBN (0.0098 g, 0.05 mmol) was refluxed in CCl_4 for 10 h. After cooling to room temperature, the solvent was evaporated under high vacuum and dissolved in methylene chloride. The organic phase was washed with water and dried over Na_2SO_4. The solvent was evaporated to give the crude product, which was then column chromatographed on silica gel, eluting with methylene chloride and hexane, to provide the desired product. Yield: 0.168 g, 48%. ^{1}H NMR (300 MHz, $CDCl_3$): δ (ppm) 8.20 (d, 9 Hz, 4H), 7.86–7.75 (m, 5H), 7.67–7.62 (d, 2H), 7.59–7.56 (d, 4H), 7.52–7.47 (t, 4H), 7.38–7.33 (t, 4H), 4.67 (s, 2H).

9,9′-(2-Azidomethyl)biphenyl-4,4′-diyl)biscarbazole (5). A mixture of **4** (2 g, 3.46 mmol) and NaN_3 (2.25 g, 34,6 mmol) in DMF was stirred at 70 °C for 10 h. After cooling to room temperature, the solvent was evaporated under high vacuum and dissolved in methylene chloride. The organic phase was washed with water and dried over Na_2SO_4. The solvent was evaporated to give the crude product, which was column chromatographed on silica gel, eluting with methylene chloride and hexane, to provide the desired product. Yield: 1.58 g, 85%. ^{1}H NMR (300 MHz, $CDCl_3$): δ (ppm) 8.28 (d, 9 Hz, 4H), 7.91–7.80 (m, 5H), 7.69–7.65 (d, 2H), 7.58–7.55 (m, 4H), 7.52–7.33 (t, 8H), 4.70 (s, 2H).

9,9′-(2-((4-Phenyl-1,2,3-triazol-1yl)methyl)biphenyl-4,4′diyl)-biscarbazole (6; CBP-TA). A mixture of **5** (3 g, 5.56 mmol), phenyl acetylene (0.68 g, 6.67 mmol), copper(II) sulfate penta-hydrate (0.42 g, 1.67 mmol) and L-ascorbic acid sodium salt (0.33 g, 1.67 mmol) in THF and water was stirred at 100 °C for 15 h. After cooling to room temperature, the solvent was evaporated under high vacuum and dissolved in methylene chloride. The organic phase was washed with water and dried over Na_2SO_4. The solvent was then evaporated to give the crude product, which was column chromatographed on silica gel, eluting with methylene chloride and hexane, to provide the desired product. Yield: 1.5 g, 42%. ^{1}H NMR(300 MHz, $(CD_3)_2CO$): δ (ppm) 8.53 (s, 1H), 8.27 (t, J = 6 Hz, 4H), 7.80 (t, J = 6 Hz, 6H), 7.75 (s, 1H), 7.72 (s, 1H), 7.57–7.48 (m, 8H), 7.45–7.71 (m, 8H), 5.93 (s, 2H). ^{13}C NMR (125 MHz, $CDCl_3$): δ (ppm) 146.41, 140.05, 139.69, 139.24, 137.95, 136.63, 136.35, 135.45, 132.07, 130.76, 130.60, 128.80, 127.83, 126.64, 126.61, 126.24, 126.08, 125.136, 122.90, 122.79, 121.98, 120.59, 120.52, 120.33, 120.14, 109.78, 109.67, 51.26. MALDI-TOF MS calc. for $C_{451}H_{31}N_5$: 641.25 g mol^{-1}, found: 641.28 g mol^{-1}. HRMS (FAB) calc. for $C_{451}H_{31}N_5$: 641.2579 g mol^{-1}, found: 641.2579 g mol^{-1}.

Acknowledgements

This work was supported by the Basic Science Research Program through the National Research Foundation of Korea (NRF) grant funded from the Ministry of Education, Science and Technology (MEST) of Korea for the Center for Next Generation Dye-Sensitized Solar Cells (no. 2010-0001842), the Samsung SDI-SNU grant and the Seoul R&BD Program (10543). We acknowledge the BK21 fellowship grants to J. K. and T.-H. K.

References

1 C. W. Tang and S. A. VanSlyke, *Appl. Phys. Lett*., 1987, **51**, 913.
2 C. W. Tang, S. A. VanSlyke and C. H. Chen, *J. Appl. Phys*., 1989, **65**, 3610.
3 J. H. Burroughes, D. D. C. Bradley, A. R. Broun, R. N. Marks, K. Mackay, R. H. Friend, P. L. Burn and A. B. Holmes, *Nature*, 1990, **347**, 539.
4 M. A. Baldo, M. E. Thompson and S. R. Forrest, *Nature*, 2000, **403**, 750.
5 (*a*) M. A. Baldo, D. F. O'Brien, Y. You, A. Shoustikov, S. Sibley, M. E. Thompson and S. R. Forrest, *Nature*, 1998, **395**, 151; (*b*) Watanabe, S. Ide and N. Kido, *Jpn. J. Appl. Phys*., 2007, **46**, 1186.
6 K. Okumoto, H. Kanno, Y. Hamaa, H. Takahashi and K. Shibata, *Appl. Phys. Lett*., 2006, **89**, 063504.
7 X. H. Zhang, M. W. Liu, O. Y. C. S. Lee, H. L. Kwong, S. T. Lee and S. K. Wu, *Chem. Phys. Lett*., 2003, **369**, 478.
8 C. H. Chuen and Y. T. Tao, *Appl. Phys. Lett*., 2004, **85**, 4609.
9 (*a*) R. J. Holmes, S. R. Forrest, Y.-J. Tung, R. C. Kwong, J. J. Brown, S. Garon and M. E. Thompson, *Appl. Phys. Lett*., 2003, **82**, 2422; (*b*) Tokito, S. Iijima, T. Suzuki, Y. Kita, H. Tsuzuki and T. Sato, *Appl. Phys. Lett*., 2003, **83**, 569.
10 (*a*) J. M. Hancock, A. P. Gifford, Y. Zhu, Y. Lou and S. A. Jenekhe, *Chem. Mater*., 2006, **18**, 4924; (*b*) T. H. Huang, J. T. Lin, L. Y. Chen and C. C. Wu, *Adv. Mater*., 2006, **18**, 602.
11 C. C. Wu, Y. T. Lin, K. T. Wong, R. T. Chen and Y. Y. Chien, *Adv. Mater*., 2004, **16**, 61.
12 J. Kwon, T.-H. Kwon, H. S. Cho, M. K. Kim, I.-S. Shin, D.-Y. Shin, S. J. Park and J.-I. Hong, *New J. Chem*., 2008, **32**, 1368.
13 S. J. Su, H. Sasabe, T. Takeda and J. Kido, *Chem. Mater*., 2008, **20**, 1691.
14 M.-H. Tsai, H.-W. Lin, H.-C. Su, T.-H. Ke, C.-C. Wu, F.-C. Fang, Y.-Li. Liao, K.-T. Wong and C.-I. Wu, *Adv. Mater*., 2006, **18**, 1216.
15 C. Adachi, R. C. Kwong, P. Djurovich, V. Adamovich, M. A. Baldo, M. E. Thompson and S. R. Forrest, *Appl. Phys. Lett*., 2001, **79**, 2082.
16 S. Tao, C. S. Lee, S. T. Lee and X. Zhang, *Appl. Phys. Lett*., 2007, **91**, 013507.
17 J. H. Lee, H. H. Tsai, M. K. Leung, C. C. Yang and C. C. Chao, *Appl. Phys. Lett*., 2007, **90**, 243501.
18 Y. Y. Noh, C. L. Lee and J.-J. Kim, *J. Chem. Phys*., 2003, **118**, 2853.

